Egypt. J. Chem. **Vol. 64,** No. 3 pp. 1371 - 1385 (2021)

Egyptian Journal of Chemistry

http://ejchem.journals.ekb.eg/

Kinetic Studies on the Adsorption of Uranium on a Mesoporous Impregnated Activated Carbon

E. A. Haggag [a], M. B. Masod [b], A. A. Abdelsamad [a,*], M. M. Abdel Aal [a], M. A. Ebiad[b]

[a] *Nuclear Materials Authority, P.No. 530 El-Kattamia, El-Maadi, Cairo, Egypt*

[b] *Egyptian Petroleum Research Institute, El-Zohour Region, Nasr City, Cairo, Egypt*

Abstract

A highly porous phosphorous-containing activated carbon derived from pistachio nutshells (PNS) was synthesis as a potential sorbent for uranium (VI) from sulfate media. The prepared phosphate activated carbon (PAC) was visualized under SEM and TEM which revealed a highly porous structure. The extraction of U(VI) from acidic media using PAC was investigated by a batch method and various parameters such as pH, equilibrium contact time, liquid to solid ratio, and initial U(VI) concentration were examined. Under the stated conditions, the optimum pH for U(VI) adsorption was found to be 3.5. The adsorption capacity of uranium upon PAC under the optimum conditions was found to be 335 mg/g. The experimental results were applied for Langmuir, Freundlich, Temkin, and Dubinin-Radushkevich (D-R) isotherm models. The thermodynamic equilibrium constant and the Gibbs free energy were determined (ΔG° from –4.72 to –7.65 kJ/mol) and results indicated the spontaneous nature of the adsorption process. Kinetics data were best described by pseudo second-order model.

Keywords: Pistachio nutshells; Uranium extraction; highly acidic solution; Phosphorous-containing activated carbon.

1. Introduction

Suitable handling of nuclear wastes has become one of the big challenges today due to their hazardous environmental effects and their potentials health effects [1]. Removal of heavy metals from nuclear waste solutions has raised a global concern in recent years [2, 3]. Uranium is considered one of the most dangerous metals [4], due to its ability to pass the living cell wall, which might lead to mutagenesis or cancer [5]. Disposal of heavy metals by adsorption process [6] is considered an effective way with advantages such as high efficiency, simplicity of design and application, being inexpensive, low sensitivity to toxic substances, and avoiding the production of toxic sludge. Activated carbon has some characteristics such as highly developed porosity, superb adsorption capacity, and a high degree of surface reactivity which make it unique [7]. Modification of activated carbon could be performed through two different processes: physical activation and chemical activation. The physical activation process is carried out in two steps which the first step is the carbonization of carbonaceous material. Additionally, in the second step, in which a high temperature is required, the activation occurs in the presence of activating agents such as CO2 or steam occurs. In comparison, the chemical activation process is a single step method in which carbonization and activation proceed simultaneously. The chemical activation offers some advantages over physical activation, including chemical activation can occur at lower temperatures, so it needs less energy and impregnation of precursor materials with the chemical agents inhibits tar formation, which results in a better transformation of the material to carbon. In other words, the carbon efficiency in a chemical method is significantly higher than the physical one [8]. Essentially, chemical activation is essential because the surface modification with proper environmentally-friendly chemicals not only will increase the adsorption capacity but will also add selectivity to carbon characteristics [9]. A lot of materials (i.e., H2SO4, H3PO4, FeCl3, and ZnCl2) have been used as chemical agents, and although ZnCl2 is widely used nowadays also it is not suitable for pharmaceutical and food industries due to its environmental problems [10]. Attia et. al [11],

*Corresponding author e-mail: Ahmed_smd@hotmail.com.

Receive Date: 21 November 2020, Revise Date: 11 December 2020, Accept Date: 20 December 2020

DOI: 10.21608/EJCHEM.2020.50611.3039

prepared pistachio shells activated by Phosphoric acid with a highly porous activated carbon and its porosity is further enhanced by prolonged soaking, the carbons produced were tested in batch experiments for the removal of two cationic dyes. According to the multitude variety of agricultural wastes in different regions, novel and inexpensive adsorbents have been manufactured to be used in industries. Various materials like olive bagasse, potato peel, soybean straw, nutshells, and a lot of other agricultural wastes have been applied to produce activated carbon [12-14].

The main idea in this work is the preparation of H3PO4-activated carbon from pistachio nutshell with high surface area and highly micro-mesoporosity for adsorption of uranium (VI) from an acidic solution. The Fourier transform infrared spectroscopy (FT-IR), surface chemistry, thermal analysis, morphological characterization by scanning electron microscopy (SEM) and High-resolution transmission electron microscopy (HRTEM), surface area, and pore structure were studied. Also, adsorption kinetics and isotherm models for the adsorption of uranium by PAC were studied.

2. Materials and methods

2.1. Preparation of PAC

Pistachio nutshell (PNS) was collected from the local markets of Cairo, Egypt. PNS was washed several times with hot distilled water to remove any adherent impurities and then dried at 105 °C for 24 hours in a vacuum drying oven. The PNS was then mixed with phosphoric acid (Extra pure, 85 %) at room temperature with a weight ratio of 1:3 (PNS: H_3PO_4) and occasional stirring for 3 days. Next, the treated Nut shell dried at 105 °C in the vacuum oven dryer. The treated PNS was then activated for 2 hours at 600 °C (at a rate of 10 °C/min) under continuous nitrogen flow (100 mL/min) in a tubular electric furnace (Nabertherm, Labothem Model R50/250/12). The produced activated sample was allowed to cool to room temperature under the same N_2 flow. Finally, the produced sample was finely grounded in an agate mortar and then washed several times with deionized water and completely dried at 110 °C, the obtained sample was designated as PAC.

2.2. Characterization of PAC

Surface morphology and microstructure of the adsorbent PAC was examined by scanning electron microscopy (SEM, JSM-5500, JEOL Ltd., Japan). The sample was coated with a thin layer of gold before SEM imaging. High-resolution transmission electron microscopy (HRTEM, JEOL 2100F TEM) was utilized to visualize the micro/mesoporosity of PAC. The textural properties of the prepared PAC were determined using N_2 adsorption-desorption isotherms at -196 °C using NOVA2000 gas sorption analyzer (Quantachrome, USA). Before analysis, the PAC was degassed overnight at 150 °C under a vacuum.

Thermal behavior of PNS and PAC was investigated using a thermogravimetric analyzer (TGA, D-50, Shimadzu, Japan) at a nitrogen flow rate of 20 mL/min and a heating rate of 10 °C/min up to 1000 °C. Fourier transform infrared spectroscopy (FT-IR) was determined using a Perkin-Elmer 1720 spectrometer in the range 400 and 4000 cm^{-1}. The samples were mixed with KBr (1:500 ratios) then pressed under vacuum. The solution pH was determined using the Jenway pH meter (Model 3510, UK). 1 g of the adsorbent in 100 mL of preboiled distilled water was shaken for 48 h; then filtered and the pH was then measured. The pH_{pzc} was also measured as reported elsewhere [15]. Bulk contents of C, H, S, and N in the samples were analyzed by a 2400 Series elemental analyzer (Perkin Elmer). Ash content and moisture of prepared PAC were determined according to ASTM D-1102 and ASTM E 871, respectively.

2.3. Equilibration Studies

Unless otherwise stated, batch adsorption experiments were performed by shaking 0.1 g of PAC with 10.0 ml of the acidic aqueous solution containing uranium. After equilibration and phase separation, the uranium concentration in the aqueous phase (Ceq, mg/L) was determined by the spectrophotometric method based on chromogenic agent Arsenazo III at 656 nm. Absorbance was measured with a UV–Visible spectrophotometer (Shimadzu UV–VIS-1601 spectrophotometer). The uranium adsorption efficiency percentage (%) was calculated according to Equation (1),

$$\text{U adsorption efficiency}\,(\%) = \frac{C_o - C_e}{C_o} \times 100 \qquad (1)$$

Where C_o and C_e are the initial and equilibrium uranium concentration in solution (mg/L), respectively. The amount of uranium adsorption q_e (mg/g) was calculated from the difference of uranium concentration in the aqueous solution at the equilibrium time according to Equation (2),

$$q_e = (C_o - C_e) \times \frac{V}{m} \qquad (2)$$

where V is the volume of solution (L), m is the weight of the resin (g). The distribution coefficient (K_d) of uranium between the aqueous bulk phase and the solid phase was calculated from the following Equation (3),

$$K_d = \frac{C_o - C_e}{C_e} \times \frac{V}{m} \quad (3)$$

2.4. Elution studies

Elution of uranium from the loaded PAC was studied using various eluting mediums such as; HCl, H_2SO_4, Na_2CO_3, HNO_3, NaOH, Na_2SO_4, CH_3COONa, and NaCl. The elution experiments were conducted by shaking 0.1 g of the loaded adsorbent with 10 mL of different eluates each separately for 60 minutes at 250 rpm. After filtrating the adsorbent, the eluting solution was analysed against uranium.

3. Results and discussion

3.1. Analysis of PAC

Elemental analysis of PNS and PAC is shown in Table 1. For PAC sample, it is clear that prepared PAC has higher contents of carbon and lower contents of oxygen, hydrogen and nitrogen compared to the raw material (PNS), this resulted due to H3PO4 activation has the dehydration effect and polymeric deformation. Also, the phosphoric acid activation led to decrease H/C ratio from 0.14 in PNS sample to 0.03. Moreover, The O/C ratio decreased from 0.97 in PNS sample to 0.25 in the PAC sample [16].

SEM images of PAC are shown in Figures 1a and 1b. SEM images illustrated irregular structure with cracks and crevices on the surface of the activated carbon and some grains in various sizes in large holes. This confirmed amorphous and heterogeneous structures. The chemical activation process was found effective in creating a large surface area with well-developed pores with different sizes shapes on the surface of pistachio nutshell activated carbon. Moreover, these pores are considered as channels to the microporous network.

TEM images for PAC are shown in Figures 1 (c–f). It is observed that The structure of the prepared activated carbon were consisting from pores structure with different sizes mainly in micropore level, which also interconnected with each other to form the internal microporous network. The porous structure was formed by the disordered packing of carbon sheets (graphitic layers with randomly arranged) and clusters. TEM image revealed clearly the micro/mesoporous structure and also confirm the nature of the amorphous structure [17].

Table 1. Elemental analysis of PNS and PAC.

Material	C %	H %	N %	S %	O % (by difference)	H/C	O/C
PNS	47.30	6.41	0.20	0.24	45.85	0.14	0.97
PAC	78.21	2.00	0.43	0.01	19.40	0.03	0.25

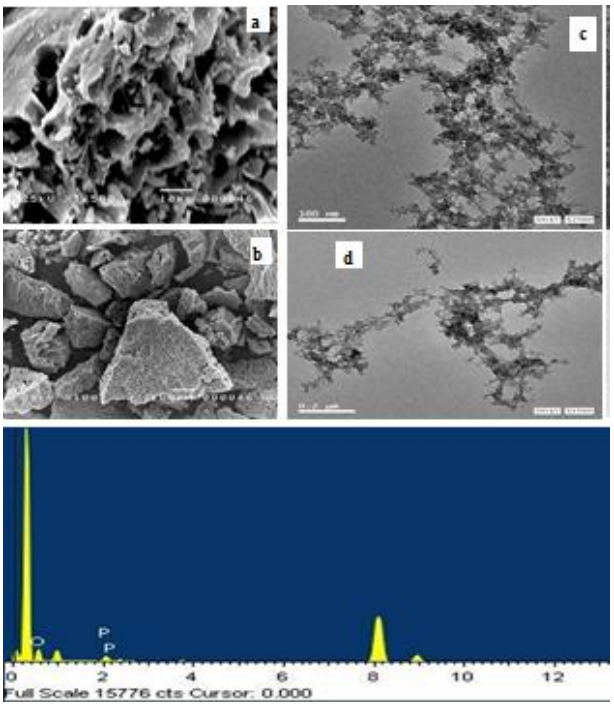

Figure 1. (a), (b) SEM, (c-f) TEM images, and (g) TEM-EDX analysis of PAC.

The occurrence of phosphorous was confirmed by TEM-EDX analysis as shown in Figure 1g. The physical and chemical properties of PNS and PAC were shown in Table 2.

Table 2. Physical and chemical properties of PNS and PAC.

Material	Bulk density (g/mL)	Moisture content (%)	Ash content	pH	pH_{PZC}
PNS	0.689	2.4	1.08	6.57	6.46
PAC	0.307	9.6	4.95	3.12	2.98

3.2. Textural analysis

The surface area and pore structure of the prepared PAC calculated from the N_2 adsorption/desorption technique are illustrated and summarized in Table 3. The adsorption isotherms of the adsorbent were the mixture of type I and IV according to IUPAC classification [18]. At low relative pressures, the sharp increase in volume indicated adsorption in micropores as in type I isotherm. While type IV with H_4 hysteresis loop appeared at intermediate and high relative pressures, indicated monolayer-multilayer adsorption followed by capillary condensation in narrow slit-like pores. These indicate that the PAC

has a mixture of the microporous and mesoporous adsorbent.

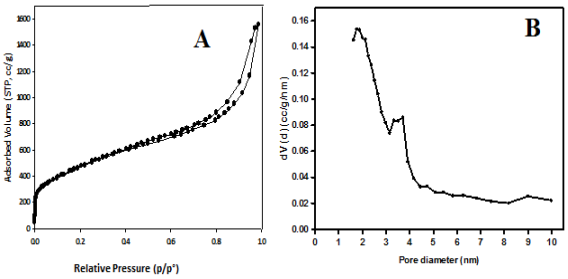

Figure 2. N_2 sorption isotherm (A) and pore size distribution (B) of PAC.

Specific surface area S_{BET} (m^2/g) was calculated from the linear plot of the BET equation, micropore surface area S_μ(m^2/g) and micropore volume V_μ (cc/g) were calculated using the t-plot method. The total pore volume V_T(cc/g) corresponding to the volume of N_2 near saturation at $p/p^o \approx 0.95$. The S_{BET} and S_μ for PAC were 1668.3 m^2/g and 1195.9 m^2/g and the micropore surface area represented 71.7 % of the total surface area. Also, the V_T and V_μ were 2.375 cc/g and 0.6622 cc/g. Moreover, the V_μ is 27.9 % of the total pore volume. The micropore diameter of the PAC was 1.81 nm while the mesopore diameter (r^-, nm) was calculated according to the following Equation (4),

$$r^-(nm) = \frac{2V_T\,(mL/g)}{S_{BET}\,(m^2/g)} \times 10^3 \qquad (4)$$

The pore size distribution of PAC showed the micro/mesoporosity (Figure 2b). Actually, the behavior of pistachio nutshell with phosphoric acid creates a high surface area and allows the development of both micropores and mesopores in the activated carbon [19].

Table 3. Textural parameters of PAC.

S_{BET} (m^2/g)	S_{mic} (m^2/g)	S_{mes} (m^2/g)	S_{mic}/S_{BET} (%)	V_T (cc/g)	V_{mic} (cc/g)	V_{mic}/V_T (%)	d_{mic} (nm)	r^- (nm)
1668.3	1195.9	472.4	71.7	2.375	0.6622	27.9	1.81	3.7

3.3. Thermal analysis

The thermal analysis decomposition behavior of the biomass (related to the chemical composition and chemical bonding in the material structure) is essentially determining the shape of the TGA profile. TGA profile of the pistachio nutshell and PAC were shown in Figure 3a. The TGA profile of the pistachio nutshell shows 10.2 wt% weight loss at 150 °C corresponds to the removal of physically adsorbed water. The weight loss between 250 and 400 °C may be attributed to the decomposition of cellulose and hemicellulose and removal of condensable gasses (methanol, acetic acid, and wood tar) and incondensable gasses (H_2, CH_4, CO, CO_2, and H_2O). And the weight loss in the range 420-700 °C can be assigned to lignin's decomposition. There is no change in weight loss over 750 °C, where the lignocellulose structure was completely decomposed. On the other hand, the TGA profile of PAC showed 13.5 % weight loss at about 150 °C related to desorption of adsorbed moisture. The physically adsorbed water over PAC is more than in raw material due to the high surface area of PAC and the presence of hydrophilic C-O functional groups [20,21]. Then, there is no variation in the TGA profile up to 750 °C.

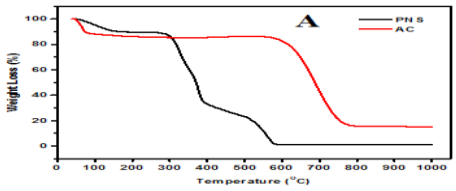

Figure 3. Thermal behaviors of PNS and PAC

3.4. Surface chemistry

The surface chemistry of carbon materials is determined by the acidity and basicity of their surface. Table 2 shows the values of pH for adsorbents and the values of pH_{pzc}. The pH of PAC is 3.12. This indicates that these acidic functional groups are predominating largely on this carbon surface [22]. One of the most important characteristics of carbon adsorbents is pH_{pzc}, which shows the point at which the adsorbent surface charge density is zero. When the pH value of the solution is less than pH_{pzc} the adsorbent reacts as a positively charged surface and when it is greater than pH_{pzc} the adsorbent functions as a negatively charged surface. The amount of pH_{pzc} obtained in this research was 2.98, this low pH_{Pzc} value also showed the dominance of acidic groups on the surface of the activated carbons. The pH_{pzc} value indicates that carbon produced from phosphoric acid activation is acidic and classified as L-Carbon [23].

The chemical structure of pistachio nutshells, phosphoric acid-activated carbons is given in Table 1. For PAC, it is clear that the PAC it has higher contents of carbon and lower contents of oxygen, hydrogen, and nitrogen compared to the raw material (PNS). This is resulted due to that H_3PO_4 activation has the dehydration effect and polymeric deformation. Also, the phosphoric acid activation led to a decrease in H/C ratio from 0.14 to 0.03 for PNS

[24]. Moreover, The O/C ratio decreased from 0.97 for PNS and to 0.25 for PAC [25].

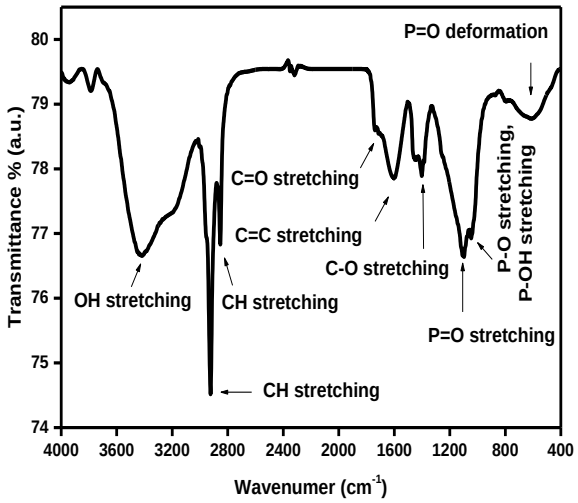

Figure 4. FT-IR spectrum of PAC.

Figure 4 proves the FTIR spectrum of PAC. The spectra revealed that the broadband located around 3415 cm^{-1} which could be assigned to the -OH stretching vibration mode of hydroxyl functional groups [26,27]. The two strong peaks located at 2853 and 2923 cm^{-1} were related to C-H stretching vibration for $-CH_2-$ and $-CH_3$. The bands at 1745 and 1716 cm^{-1} were corresponding to C=O stretching vibration in the carboxylic group. The bands at 1450, 1438, 1400, and 1385 cm^{-1} were assigned to C-O stretching in carboxylate groups. Also, The stretching vibrations of $-CH_3$ at 1385 cm^{-1} was related to methyl structures [20]. The broadband around 1300 and 900 cm^{-1} with maxima at 1100 and 1046 cm^{-1}, respectively was found with oxidized carbons and has been assigned to C-O stretching in acids, alcohols, phenols, ethers, and/or esters groups [28]. Nevertheless, it is also a characteristic of phosphorous and phosphor carbonaceous compounds present in the phosphoric acid activated carbons [29]. Assignment in this region is difficult because absorption bands are overlapped. The peak at 1190-1200 cm^{-1} may be also assigned to the stretching mode of hydrogen-bonded P-O, to O-C stretching vibrations in P-O-C linkage, and POOH [30]. The shoulder at 1100 cm^{-1} was ascribed to ionized linkage P^{+}-O^{-} in acid phosphate and symmetrical vibration in a P-O-P chain [31].

Surface acidity and basicity is a crucial factor for describing the chemistry of the carbon adsorbent surface. In the current research, the acidity and basicity of PAC were calculated to be 1.831 and 0.081 meq/g, respectively. Results prove the acidity nature of PAC surface which is due to the presence of oxygen-containing groups like phosphate group, while basicity could be a result of the presence of oxygen-free Lewis sites, like carbonyls [22]. Observing a higher level of surface acidity than basicity for carbon adsorbent surface agrees with results concluded from pH_{pzc} value. Also, the phosphoric acid activation leads to creates a new phosphate group [32], which will enhance its sorption toward the removal of the uranium from the aqueous solution [33].

3.5. Extraction of Uranium by using PAC

The factors that affect the sorption efficiency of uranium from solution using the solid-liquid batch technique were studied. The relevant factors included:

3.5.1. pH effect

The effect of pH on the adsorption efficiency of U(VI) was studied in Figure 5. From the obtained data, it is clearly obvious that there is a significant increase of the adsorption efficiency from pH of 1.0 up to 3.5 with about 96.3 % uranium adsorption, and then the adsorption efficiency was decreased significantly. The highest and lowest adsorption efficiency was 96 and 16% at a pH of 3.5 and 1.0, respectively. The high adsorption rate in the acidic region could be explained by the presence of anionic species of uranium and also the carbon surface charge as follows: So the electrostatic force between the negatively charged uranium species such as $(UO_2(SO_4)_2^{-2}$ and positively charged functional groups on the adsorbent surface easily adsorbs the anions in solution. Therefore, in acid regions the adsorption is higher; however, increasing pH may lead to a neutral functional group on carbon adsorbent surface. Phosphate groups on carbon surface at lower pH $(PAC\text{-}H\text{-}H_3PO_4)^{+}$ are protonated. Increasing the pH value results in the subsequent formation of the neutral form $(PAC\text{-}(H_3PO_4)°)$ and ionized $(PAC\text{-}H_2PO_4^{-})$ which weakens the electrostatic attraction between functional groups and uranium anionic species which leads to less U(VI) removal [34].

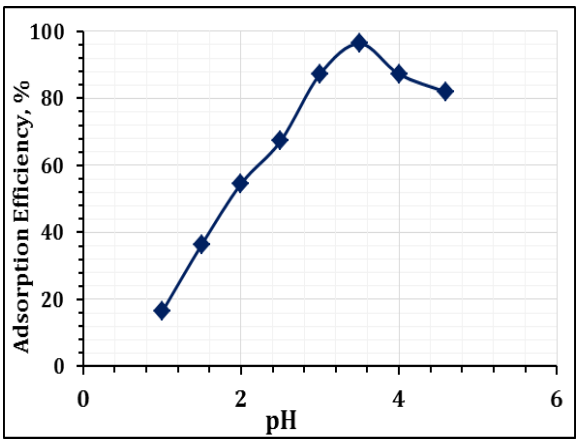

Figure 5. Influence of pH on the adsorption efficiency of U(VI).

3.5.2. Effect of contact time

Figure 6 shows that the effect of contact time (from 5 to 120 minutes) on the adsorption of uranium by PAC. From the graph, it has been observed that uranium adsorption was gradually increased by increasing the contact time from 5 to 90 min to reach the optimum adsorption after 90 minutes. This attained time was considered as adsorption equilibrium time, then after this time, the interval adsorption process has been the same. This is because at the beginning of the process numerous vacant surface sites are available to be filled with uranium, therefore the adsorption process is faster, however when lots of active sites are covered, repulsive forces between the absorbed ions and the remaining ions in the solution becomes considerable and it causes a delay in reaching the equilibrium time.

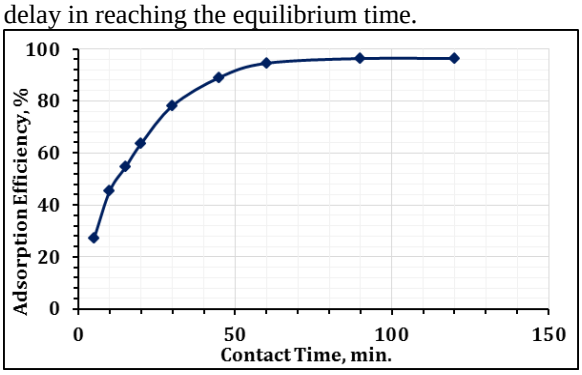

Figure 6. Influence of contact time on the adsorption efficiency of U(VI).

3.5.3. Effect of solid to liquid ratio

The effect of solid to liquid ratio on adsorption efficiency of uranium investigated by adding different amounts of PAC ranged from 0.01 to 0.10 g to 10 ml volume of uranium solution, its conc. 550 mg/L, and agitating for 90 minutes at room temperature 25±1 °C. The obtained result was given in Figure 7. From the graph, it is found that the adsorption efficiency of uranium increased from solid to liquid ratio 0.01:10 to 0.1:10. Accordingly, the preferred liquid to solid ratio is at 0.01:10 ratios which give 60.9 % adsorption efficiency while the corresponding uptake was 335 mg U/g.

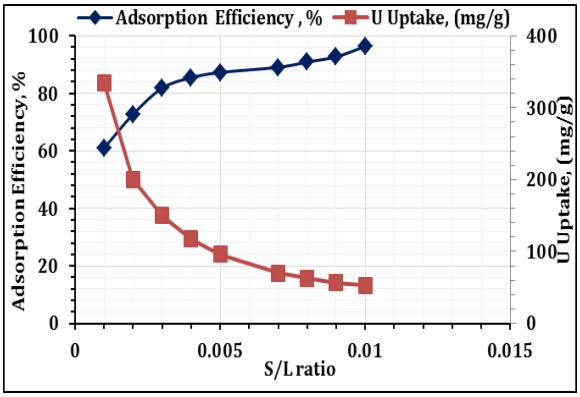

Figure 7. Influence of solid to the liquid ratio on the adsorption efficiency of U(VI).

3.5.4. Effect of uranium initial concentration

The performance of uranium adsorption on PAC was investigated as a function of the initial uranium concentration (400 - 8000 mg/L) at a pH value of 3.5 and 0.1 gram of adsorbent for 90 min. The effect of the initial concentration of uranium on the adsorption efficiency is presented in Figure 8. The uranium adsorption was increased by increasing the uranium concentration from 400 to 8000 mg/L with the corresponding uptake of 38 to 337 mg U/g, while adsorption efficiency decreased. This is due to the increase in the concentration of uranium the number of active sites on the PAC saturated by uranium increased which indicates the high affinity of the uranium complex to bond with the active sites present on the modified PAC. Thus, the maximum adsorption capacity of PAC was 337 mg U/g adsorbent.

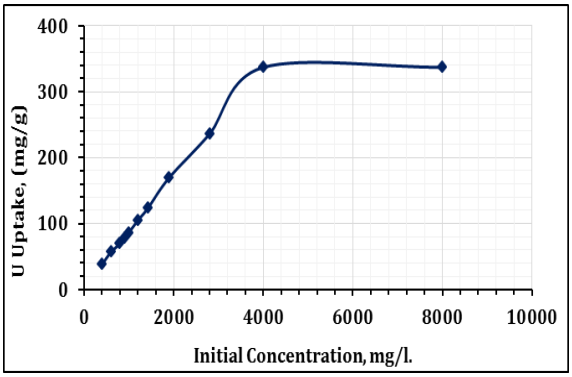

Figure 8. Influence of initial uranium concentration on the adsorption efficiency of uranium (VI).

3.5.5. Uranium adsorption kinetics

Figure 9 represents the kinetic profiles of uranium adsorption onto PAC at different contact times and at four different temperatures (25, 30, 40, and 50 °C). The results showed that, for all initial concentrations, the uranium adsorption was fast increase and then slowed down until equilibrium was achieved. For PAC adsorption equilibrium attained in the first 90 min at the four different temperatures, From 0 to 90 min, the uptake increase sharply due to the availability of free active sites on the adsorbent surface and high concentration of U(VI). After that period, very few free active sites on the adsorbent surface are available, hence, we observed a slow increase in U(VI) adsorption. The quick kinetics has significant practical and economic importance for PAC for the high concentration of U(VI), as it facilitated smaller reactor volumes, confirming high efficiency and economy [34].

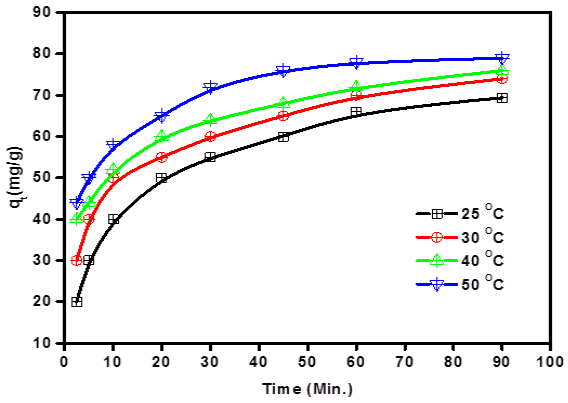

Figure 9. Effect of time on U(VI) adsorption by PAC at 25, 30, 40, and 50 °C (initial concentration 550 mg/L, pH = 3.5).

To estimate the adsorption rate for uranium, four kinetic models and two adsorption mechanisms were considered. The kinetic models used to investigate the mechanism of adsorption were the pseudo-first order [35], pseudo-second order kinetic models [36], intraparticle diffusion models [37], and Boyd model [38].

The pseudo-first-order model is given by Lagergren as [35]:

$$\log (q_{e1} - q_t) = \log q_{e1} - (\frac{k_1}{2.303})\, t \qquad (5)$$

where q_e and q_t are the amounts of uranium adsorbed at equilibrium and time t (mg/g), and k_1 is the rate constant of pseudo first-order adsorption process (min^{-1}). The values of the first-order rate constant k_1 and equilibrium adsorption capacity q_e were estimated from the slope and intercept of plotting log (q_e-q_t) against t. The kinetic parameter of adsorption of uranium summarized in Table 4, the correlation coefficient (R^2) values for the pseudo-first-order kinetic are ranged from 0.9781 to 0.9957, however, there was a large difference in q_e between the experimental and calculated values, suggesting a poor fit for the pseudo-first-order kinetic model to the experimental data.

The pseudo-second-order kinetic model by McKay and Ho [36] expressed as:

$$\frac{t}{q_t} = \frac{t}{q_{e2}} + \frac{1}{k_2 q_{e2}^2} \qquad (6)$$

Additionally, qe_2 U(VI) adsorption over PAC were 75.19, 77.52, 78.74 and 81.92 mg/g at 25, 30, 40 and 50 °C, respectively. The high adsorption rate of PAC is attributed to the presence of high oxygenated groups and high surface area reached at 1668.3 m^2/g moreover the majority of pores attributed to microporous in nature.

Where k_2 is the pseudo-second-order rate constant (g/mg min) and can be determined experimentally from the slope and intercept of plot t/q_t versus t (Figure 10). An extremely high correlation coefficient obtained was > 0.99 for all concentrations at the four different temperatures and this kinetic model provides the best agreement between the calculated values of q_{e2} and the experimental q_e data. These results suggest that the uranium adsorption mechanism on PAC obeyed the pseudo-second-order (PSO) kinetic model [39].

The intraparticle diffusion model was first recommended by Weber and Morris [37], who determined that the uptake is proportional to the square root of the contact time during the adsorption as shown in Figure 11a.

$$q_t = K_{id}\, t^{0.5} + C_i \qquad (7)$$

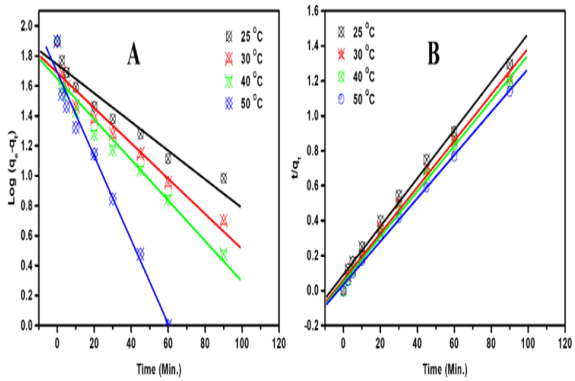

Figure 10. Pseudo first - order kinetic (A) and Pseudo-second-order (B) kinetic models for the adsorption of U(VI) onto PAC.

where K_{id} is the rate constant of intraparticle transport ($mg/g.min^{1/2}$). According to this model, the dual nature of the curves may be attributed to the difference of the adsorption extents in the initial and final stages. The first steep portion stands for the external surface adsorption, and the second portion rises gradually with the intraparticle diffusion. If the intraparticle diffusion is the rate-limiting step, the plot of q_t *vs.* $t^{1/2}$ should be linear and pass through the origin. None of the intraparticle diffusion plots passed through the origin which revealed that the intraparticle diffusion was part of the adsorption but was not the only rate-controlling step and refers to the effect of film diffusion (boundary layer diffusion). Table 4 shows the constants K_{id} and C values, it was found that the lines do not pass through the origin, accordingly, The adsorption mechanism is rather a complex process and the intraparticle diffusion is not the only controlled rate step and this indicates the effect of film diffusion on the U(VI) adsorption [40].

To predict the actual slow step involved, the kinetic data were further examined using the Boyd kinetic model to separate between film diffusion and particle

diffusion. Boyd kinetic equation [38] was applied, which is represented as.

$$F(t) = 1 - \frac{6}{\pi^2}\sum_{n=1}^{\infty}\frac{e^{-n^2Bt}}{n^2} \quad (8)$$

where, F is the fractional attainment of the equilibrium at a different time (t), and B(t) is a mathematical function of F.

$$F = \frac{q_t}{q_e} \quad (9)$$

where q_t and q_e are the amount adsorbed at a time (t) and equilibrium, respectively.

Reichenberg [41] managed to obtain the following approximations:

For F values > 0.85

$$B(t) = -0.4977 - \ln(1 - F) \quad (10)$$

And for F values < 0.85

$$B(t) = \left(\sqrt{\pi} - \sqrt{\pi - \left(\frac{\pi^2 F(t)}{3}\right)}\right)^2 \quad (11)$$

Plotting of B(t) against time t as shown in Figure 11b to investigate the linearity of the experimental value and the data listed in Table 4.

If the plots are linear and pass through origin the adsorption process is controlled by particle-diffusion mechanisms. The data indicated that the adsorption process of U(VI) onto the PAC is not controlled by film diffusion. Since the plot lines do not pass through the origin.

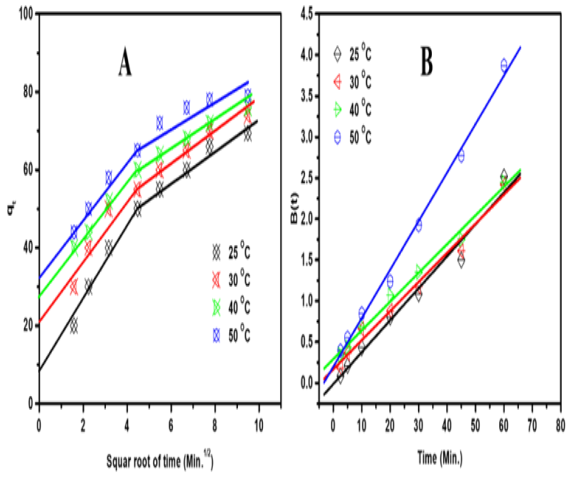

Figure 11. Intraparticle diffusion (A) and Boyd plots (B) for adsorption of U(VI) onto PAC.

Table 4. Kinetic parameters (pseudo - first order and pseudo- second order) for the adsorption of U(VI) onto PAC at different temperatures.

Model	Constant parameter	PAC			
		25 °C	30 °C	40 °C	50 °C
Experimental	$q_{e,\ exp}$ (mg/g)	69.4	74.0	76.0	79.0
Pseudo first order	q_{e1} (mg/g)	49.73	41.83	36.77	41.25
	K_1 (L/min)	0.042	0.038	0.036	0.060
	R^2	0.9789	0.9781	0.9904	0.9957
Pseudo second order	q_{e2} (mg/g)	75.19	77.52	78.74	81.92
	K_2 (g/mg min)	0.00150	0.00208	0.00256	0.00335
	R^2	0.9969	0.9958	0.9969	0.9991
Intraparticle diffusion	K_{id}	10.18	8.47	7.06	7.26
	C	5.86	19.49	28.80	33.47
	R^2	0.9771	0.9179	0.9947	0.9828
Boyd plot	Intercept	-0.013	0.167	0.292	0.200
	R^2	0.9760	09811	0.9924	09945

3.5.6. Adsorption isotherms

The adsorption isotherms play an important role to determine the maximum adsorption capacity. The amount of U(VI) adsorbed q_e (mg/g) is plotted against the equilibrium concentration C_e (mg/L) for PAC at four different temperatures, as illustrated in Figure 12. According to the isotherms shape, curves, and the Giles classification [42], the adsorption isotherm of PAC is classified as L-type. In this model, the adsorption is initially quite rapid, followed by a slow approach to equilibrium at high concentrations.

The adsorption data were investigated by fitting them to different isotherm equations of Langmuir, Freundlich, Temkin, and Dubinin-Radushkevich (D-R).

Langmuir adsorption model is the most commonly used isotherm equation. The linear form of the Langmuir isotherm equation is characterized by reference [43].

$$\frac{C_e}{q_e} = \frac{1}{bq_m} + \frac{C_e}{q_m} \quad (12)$$

where Ce (mg/L) is the equi¬librium concentration, qe (mg/g) is the amount adsorbed at equilibrium, b (L/mg) is the Langmuir constant, and qm (mg/g) represents the monolayer capacity. The maximum adsorption capacity (qm, mg/g) was estimated from the slope of the plot of Ce/qe versus Ce (Figure 12).

The obtained higher correlation coefficient (R2) which is more than 0.99 indicating a good linear fit for Langmuir's model as shown in Table 5.

Upon inspection of Table (5), (i) shows that the adsorption process is favorable for U(VI) for Langmuir's model as indicated from the high values of correlation coefficient (R2), which ranged from 0.9905 to 0.9994. (ii) The adsorption capacities of PAC at 25 °C, 30 °C, 40 °C and 50 °C were 357.14, 370.37, 384.62 and 384.62 mg/g.

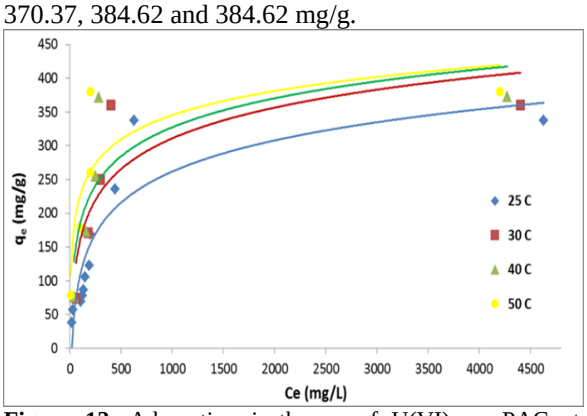

Figure 12. Adsorption isotherms of U(VI) on PAC at different temperatures.

This is due to high surface area of prepared sample (1668.3 m^2/g) and its well characteristic functional group (iii) The Langmuir adsorption constant (b) represents the affinity between the adsorbent and adsorbate. The magnitude of b has small values (0.003–0.016 L/mg) , which shows a low heat of adsorption capacity [44].

The essential characteristics of Langmuir isotherm can be configured by a dimensionless constant known as equilibrium parameter (R_L), it can be written as:

$$R_L = \frac{1}{1+b\,C_o} \qquad (13)$$

where the C_o is the highest initial U(VI) concentration present the solution (mg/L). R_L is an indicator of the favorability of an isotherm. When, $R_L > 1$ indicates unfavorable adsorption; $R_L = 1$ is for a linear adsorption; $0 < R_L < 1$ indicates favorable adsorption; and $R_L = 0$ indicates an irreversible adsorption [45]. The R_L values of the adsorption of uranium ions on PAC are reached 0.0345 at 25 °C (Table 5). This shows that the adsorption process is favorable for U(VI) by the prepared activated carbon PAC.

The Freundlich isotherm [46] is derived by assuming a heterogeneous surface with a non-uniform distribution of heat of adsorption over the surface

$$q_e = K_f\,C_e^{1/n} \qquad (14)$$

where C_e is the solute concentration in the liquid at equilibrium (mg/L), q_e is the amount of U(VI) sorbed at equilibrium (mg/g), K_F (mg/g), and n are the Freundlich constants related to adsorption capacity and adsorption intensity. The linearized form of Freundlich isotherm can be written as follows:

$$\log q_e = \log K_F + \frac{1}{n}\log C_e \qquad (15)$$

The Freundlich constant K_F and n can be calculated from the intercept and slope of a plot between log q_e and log C_e. The correlation coefficients and Freundlich constants K_F and n are represented in Table 5.

If n values lying in the range of 1-10 means favorable adsorption. The heterogeneous nature of the surface was identified by a value of 1/n the range 0-1 [47]. the values of the correlation coefficient were $R^2 <$ 0.95 From U(VI) and prepared activated carbon [48]. The result in Table 5 showed that n values for PAC and 1/n are 2.211 and 0.4523, respectively, at 25 °C. These indicate a high adsorption capacity in PAC isotherms and regression coefficients. It can conclude that the Langmuir equation indicates the best fit of experimental data over the Freundlich equation for PAC samples.

Temkin isotherm assumes that: (i) the adsorbent-adsorbate interactions lead to a linear decrease in the heat of adsorption of all the molecules in the layer with surface coverage. (ii) the adsorption is considered by a uniform distribution of binding energies, up to some maximum binding energy [49-51].

The Temkin isotherm equation represented as:

$$q_e = \frac{RT}{b}\ln(K_T\,C_e) \qquad (16)$$

This can be linearized as:

$$q_e = B_1 \ln K_T + B_1 \ln C_e \qquad (17)$$

where K_T is the equilibrium binding constant (L/mol), B_1 is related to the heat of adsorption and R is the universal gas constant (8.314 J/mol K).

The Temkin isotherm constants B_1 and K_T are calculated from the slope and the intercept of the plot of q_e versus Ln C_e as shown in Figure 13.

From Table 5, the heat of uranium adsorption (b) is corresponding to coverage of U(VI) on the prepared sample because of the adsorbent-adsorbate interaction. For PAC, it was found that slightly increased of b (from 0.884 to 1.448 KJ/mol) with increasing temperature from 298 to 313 K. This indicates that the heat of adsorption of uranium onto the surface of PAC is endothermic [52]. The values of correlation coefficient R^2 is ranged from 0.6539-0.8151 for PAC. Generally, Temkin isotherm equation poor fit compared with Langmuir.

Dubnin-Redushkevich (D-R) isotherm used to identify if the adsorption occurred is physical or chemical in nature, the equilibrium data were applied

to the D-R Equation [53]. The linearized form of the D-R model is assumed as Equation (18),

$$\ln q_e = \ln q_m - \beta\varepsilon^2 \quad (18)$$

where β is the activity coefficient related to mean adsorption energy (mol^2/J^2) and ε is the Polanyi potential. Where, The Polanyi potential [54] can be designed using the Equation (19),

$$\varepsilon = RT\ln(1+\frac{1}{C_e}) \quad (19)$$

The mean adsorption energy, E (kJ/mol) is calculated with the help of Equation (20),

$$E = \frac{1}{\sqrt{2B}} \quad (20)$$

Figure 13 indicated the plot of Ln q_e versus ε^2 should yield a straight line. The value of the D-R constants is illustrated in Table 5. From the obtained results, the values of correlation coefficient (R^2) for the PAC are ranged 0.4449-0.8545. These indicate that the D-R model is less fit than the Langmuir model. The adsorption potential is independent of the temperature, but it depends upon the nature of the adsorbent and adsorbate. As is well known, the isotherms of Langmuir and Freundlich do not establish the mechanism of adsorption. While the free energy (E) in the D-R isotherm estimate the adsorption type, when the E value is between 8 and 16 kJ/mol, indicate chemical ion exchange mechanism of adsorption; however, physical adsorption is considered when the E value is lower than 8 kJ/mol [55]. The adsorption energies (E) for investigated samples are ranged from 0.027-0.158 kJ/mol. These values indicated that the adsorption process of U(VI) onto the prepared sample is physical in nature.

3.5.7. Determination of thermodynamic parameters

Thermodynamic parameters such as Gibbs free energy (ΔG°), entropy (ΔS°), and enthalpy (ΔH°) were calculated using the following equations:

$$K_d = \frac{C_s}{C_e} \quad (21)$$

$$\Delta G^o = \Delta H^o - T\Delta S^o \quad (22)$$

$$ln\ K_d = \frac{\Delta S}{R} - \frac{\Delta H}{RT} \quad (23)$$

where K_d is the adsorption distribution coefficient, C_s the amount of uranium adsorbed on the prepared samples per liter of the solution at equilibrium, and C_e is the equilibrium concentration (mg/L) of U(IV) in the solution. T is temperature and R is the gas constant. ΔH° and ΔS° were calculated from the slope and intercept of Van't Hoff plots of ln K_d versus 1/T.

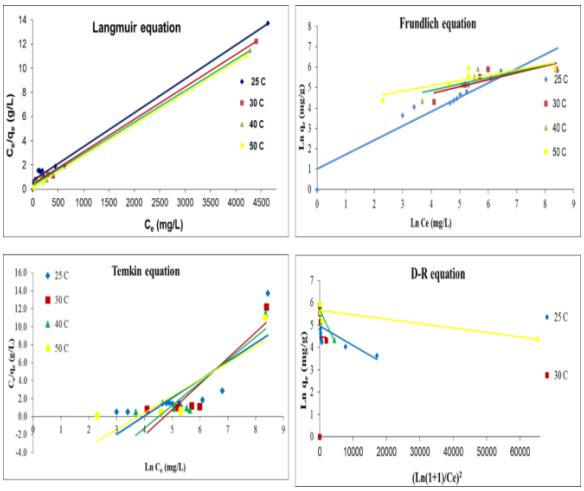

Figure 13. The linearized form of Langmuir, Frundlich, Temkin, and D-R equations for U(VI) at different temperatures.

Table 5. Parameters of adsorption isotherms for adsorption of U(VI) onto PAC at temperatures 25, 30, 40, and 50 °C.

Model	Constant parameter	25 °C	30 °C	40 °C	50 °C
Langmuir isotherm	q_m (mg/g)	357.14	370.37	384.62	384.62
	b (L/mg)	0.003	0.006	0.008	0.016
	R^2	0.9905	0.9978	0.9985	0.9994
	R_L	0.0345	0.0191	0.0153	0.0078
Freundlich isotherm	K_F (mg/g)	11.157	28.809	36.514	57.231
	n	2.211	2.955	3.186	3.821
	1/n	0.4523	0.3380	0.3140	0.2620
	R^2	0.8487	0.6580	0.6464	0.7440
Temkin isotherm	b (KJ/mol)	1.224	0.884	1.024	1.448
	K_T	0.019	0.009	0.011	0.023
	B_1	2.024	2.850	2.540	1.854
	R^2	0.6539	0.8121	0.8151	0.7172
Dubinin-Radushkevich isotherm	q_{max} (mg/g)	145.039	293.624	292.364	288.213
	β (mol^2/kj^2)	9.0×10^{-5}	7.0×10^{-4}	3.0×10^{-4}	2.0×10^{-5}
	E (kj/mol)	0.075	0.027	0.041	0.158
	R^2	0.4449	0.8545	0.8113	0.7798

Based on the values of the achieved thermodynamic parameters (Table 6), the negative values of ΔG° indicate spontaneous adsorption of U(VI) on the phosphorous-containing activated carbon. Adsorption of U(VI) can be considered as physisorption when the change in free energy for this process ranges between -4.72 and -7.65 kJ/mol because it is known that the absolute magnitude of the change in free energy for physisorption is between -20 and 0 kJ/mol and that chemisorption occurs between -80 and -400 kJ/mol [56]. It should also be noted that the change in free energy decreases with an increase in temperature, which indicates an increase in adsorption capacity with a temperature rise. The positive values of entropy change reflect the increased randomness at the solid/solution surface. This is a direct consequence of enhancement of the mobility and extent of penetration within activated carbon pores and overcoming the activation energy barrier and enhancing the rate of intraparticle diffusion. The positive values of ΔH° (28.32 kJ/mol) confirm the endothermic nature of adsorption and explain the increase in adsorption capacity of the PAC to U(VI) with a temperature increase [31].

Table 6. Thermodynamic parameters for adsorption of U(VI) onto PAC at temperatures 25, 30, 40, and 50 °C.

T (K)	ΔG° (kJ/mol)	K_d	ΔH° (kJ/mol)	ΔS° (J/mol K)
298	-4.72	6.72	28.32	111.62
303	-5.77	9.89		
313	-6.64	12.83		
323	-7.65	17.29		

3.5.8. Uranium elution

Many elution tests were performed to elute U(VI) ions from the loaded PAC after the sorption process. Different solutions such as HCl, H_2SO_4, HNO_3, NaOH, Na_2CO_3, NaCl, Na_2SO_4, and CH_3COONa were used to attain the maximum elution percent. Uranium elution experiments were performed using a batch method at room temperature. The elution experiments were occurred by shaking 0.1 g loaded PAC and 10 mL of 1 molar for eluting reagent for 1 hour at 250 rpm. Regeneration of PAC again using 1 molar phosphoric acid may be satisfactory for the regeneration of the adsorbent again. The result of uranium elution from the PAC by using different solutions was graphically plotted in Figure 14. From the obtained data, it is clearly obvious that Na_2CO_3 is the best eluent with 89.2% elution efficiency due to high selectivity of Carbonate towards uranium to form stable uranyl carbonate complex [57].

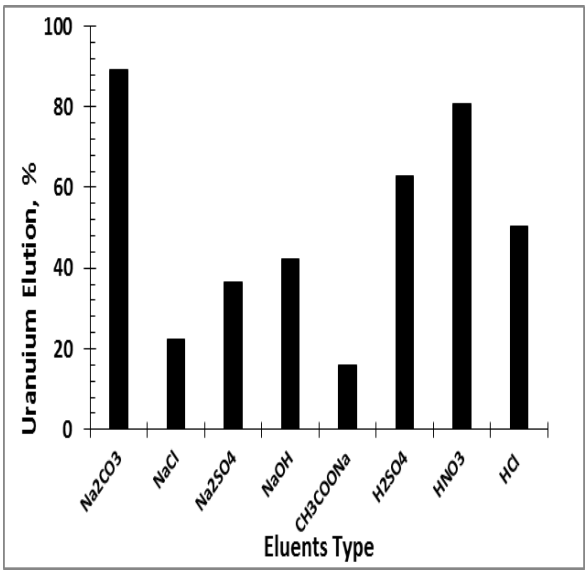

Figure 14. Effect of eluent type on a percentage of uranium elution.

3.5.9. Elemental composition of the PAC

To define the chemical composition of the PAC after loading with U(VI) ions were subjected to EDX analysis [58]. After adsorption U(VI) ions characterized by EDX showed the presence of P, O, C and U were observed suggesting the uptake of U(VI) by PAC as shown in Figure 15.

The comparison between the sorption capacity of PAC and other sorbents is given in Table 7.

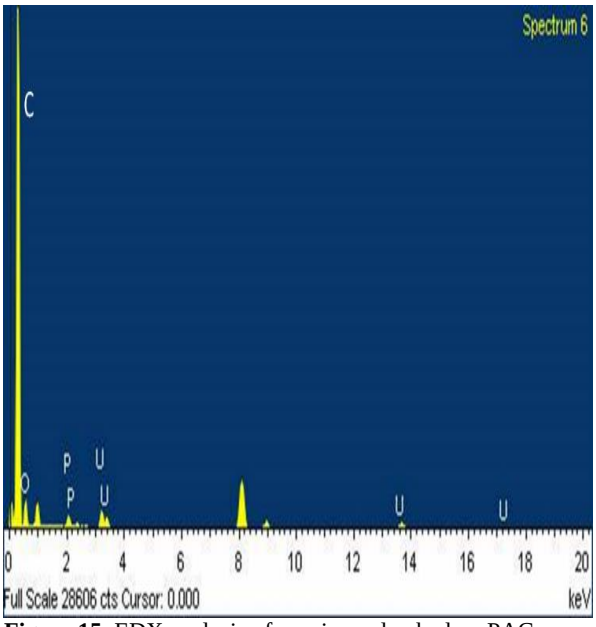

Figure 15. EDX analysis of uranium adsorbed on PAC.

Table (7): The experimental capacity of PAC compared with the sorption capacity of other sorbents:

Type	sorption capacity, (mg/ g)	References
PurolitA 400	117.6	[59]
Amberjet 1200 H	131.4	[60]
Polyurethane	75	[61]
polyethyl eniminephenyl phosphonamidic acid	39.6	[62]
succinic acid impregnated amberlite XAD-4	12.3	[63]
gel-amide	28.9	[64]
natural clinoptilolite zeolite	0.7	[65]
RHA–aluminum composite	85	[66]
PAC	337	Present work

4. Case Study: El-Sela Leach Liquor

Under the preferred conditions, the applicability of PAC for uranium (VI) ions removal from El-Sela sulfate leach liquor sample was checked. In this respect, the initial pH of the working solution was adjusted by the addition of a buffer solution. After that, 100 ml of the sample was shaking with the PAC (337 mg U/g), indicated that under the working conditions, 88 % of the theoretical capacity was realized. The decrease in the PAC capacity may be due to the competition between uranium and different ions presented in the sample (as iron ions). About (98.0%) of the loaded uranium was eluted with 1M Na_2CO solution. Uranium has been precipitated from the eluted solution using hydrogen peroxide. The precipitate was dried at 110–120 °C for 48 h and the XRF analysis for the uranium product was found to have a purity of 98.44% as shown in Figure16. All processes are shown in Figure 17, as a graphical abstract.

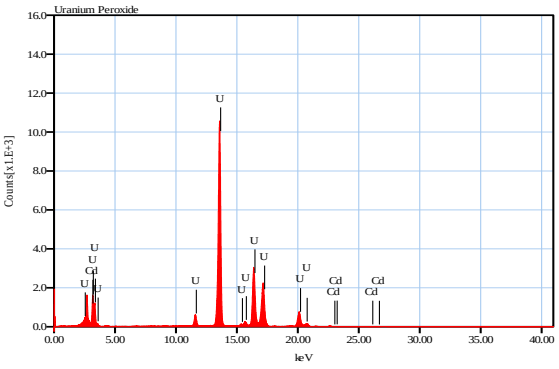

Figure 16: XRF analysis of the precipitated uranium from PAC

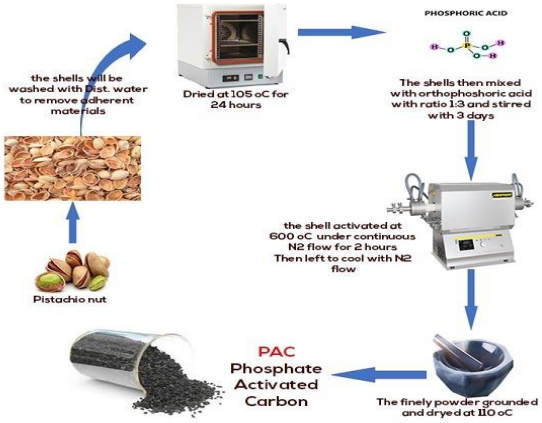

Figure 17: Graphical abstract

4. Conclusions

Preparation of PAC has been achieved from pistachio nutshells. The results of BET analysis showed that the PAC has a very high surface area and high micro/mesoporosity. Based on the conducted experiments, the optimum pH value was found to be 3.5 which indicates that PAC has a high level of activity in acidic regions. The optimum contact time and solid to liquid ratio are 90 minutes and 0.01:10. Kinetics studies stated that pseudo second-order kinetic model successfully fitted the experimental data and the rate-limiting step in the process might be the physical adsorption.

The equilibrium data were properly described by the Langmuir model, showing a maximum adsorption capacity of 337 mg/g at 25 °C. Thermodynamic studies confirmed that adsorption of U(VI) onto PAC could be considered a spontaneous, endothermic, and favorable process. Uranium elution from the loaded PAC has been investigated. The obtained results showed that about 89.2% of uranium was eluted successfully using 1 molar Na_2CO_3 solution.

Conflict of Interest:

All the authors have no conflict of interest.

References

[1] Kouraim K. M., Hagag M., S., and Ali A. H., Adsorption of uranium from its aqueous solutions using activated cellulose and silica grafted cellulose. *Radiochimica Acta*, 108 (4), 261–271(2019).

[2] Bone S. E., Dynes J. J., Cliff J. B., and Bargar J. R., Uranium(IV) adsorption by natural organic matter in anoxic sediments. *Proceeding of the National Academy of Sciences of the United States of America*, 114 (4), 711-716(2017).

[3] Sun Y., Wu Z., Xiangxue Wang X., Ding C., Cheng W., Yu S., and Wang X., Macroscopic and microscopic investigation of U (VI) and Eu (III) adsorption on

carbonaceous nanofibers. *Environ. Sci. Technol.*, 50 (8), 4459–4467(2016).

[4] Masoud A., Saeed M., Taha M., El-Maadawy M., Uranium Adsorption from Bahariya Oasis leach liquor via TOPO Impregnated Bentonite Material; Isothermal, kinetic and Thermodynamic Studies. Egypt.J.Chem., 63(2), 721-741 (2020).

[5] Mansour H., Mahmoud K., Kamal H., Mahdy H., Uranium Bio-sorption from its Processed Waste Solution by Green Algae. Egypt. J. Chem., 63 (10), 4039 - 4054 (2020).

[6] Zhao Y., Guo C., Fang H., and Jiang J., Competitive adsorption of Sr (II) and U (VI) on graphene oxide investigated by batch and modeling techniques. *J. Mol. Liq.*, 222, 263–267(2016).

[7] Deveci H. and Kar Y., Adsorption of hexavalent chromium from aqueous solutions by bio-chars obtained during biomass pyrolysis. *J. Ind. Eng. Chem*, 19, 190-196(2013).

[8] Jain A., Balasubramanian R. and Srinivasan M.P., Hydrothermal conversion of biomass waste to activated carbon with high porosity: a review. *Chem. Eng. J.*, 283, 789-805(2016).

[9] Pezoti O., Cazetta A.L., Bedin K.C., Souza L.S., Martins A.C., Silva T.L. and et al., NaOH-activated carbon of high surface area produced from guava seeds as a high-efficiency adsorbent for amoxicillin removal: Kinetic, isotherm and thermodynamic studies. *Chem. Eng. J.*, 288, 778-788(2016).

[10] Pezoti O., Cazetta A.L., Souza I.P.A.F., Bedin K.C., Martins A.C., Silva T.L. and et al., Adsorption studies of methylene blue onto $ZnCl_2$-activated carbon produced from buriti shells. *J. Ind. Eng. Chem.*, 20, 4401-4407(2014).

[11] Attia A. A., Girgis B.S., and Khedr S. A., Capacity of activated carbon derived from pistachio shells by H_3PO_4 in the removal of dyes and phenolics. *J Chem. Technol. Biotechnol.*, 78, 611–619(2003).

[12] Attia A. A., Girgis B.S., and Fathy N. A., Removal of methylene blue by carbons derived from peach stones by H_3PO_4 activation: Batch and column studies. *Dyes and Pigments*, 76, 282-289(2008).

[13] Moreno-Piraján J.C. and Giraldo L., Activated carbon obtained by pyrolysis of potato peel for the removal of heavy metal copper (II) from aqueous solutions. *J. Anal. Appl. Pyrolysis.*, 90, 42-47(2011).

[14] Miao Q., Tang Y., Xu J., Liu X., Xiao L. and Chen Q., Activated carbon prepared from soybean straw for phenol adsorption. *J., Taiwan Inst., Chem., Eng.*, 44, 458-465(2013).

[15] Puziy A., Poddubnaya O., A Martı´nez-Alonso A., Castro-Mun˜ iz A., Sua´rez-Garcı´ F., Tasco´n J., Oxygen and phosphorus enriched carbons from lignocellulosic material. *Carbon*, 45, 1941–1950 (2007).

[16] Rafiee A., Nasab S. and Teimouri A., Synthesis and characterization of pistachio shell/nano diopside nano composite and its application for removal of Crystal Violet dye from aqueous solutions using central composite design. *IJEAC*, 12, 970-982(2019).

[17] Mozaffarian M., Soleimani M. and Bajgiran A., simple novel route for porous carbon production from waste tyre. J. Environ. *Sci. Pollut. Res.*, 26, 31038-31054(2019).

[18] Sing K.S.W., Reporting physisorption data for gas solid systems with special reference to the determination of surface-area and porosity. *J. Pure Appl. Chem.*, 57, 603-619(1985).

[19] Liu Y., Yao X., Wang Z., Li H., Shen X., Yao Z. and Qian F., Synthesis of Activated Carbon from Citric Acid Residue by Phosphoric Acid Activation for the Removal of Chemical Oxygen Demand from Sugar-Containing Wastewater. *envir. engi. sci. j.*, 36(6), 656-666(2019).

[20] Yang T. and Lua A.C., Characteristics of activated carbons prepared from pistachio-nut shells by physical activation. *J. Colloid Interface Sci.*, 267 (2), 408-417(2003).

[21] László K., Bóta a.and Nagyu L.G., Characterization of activated carbons from waste materials by adsorption from aqueous solutions. *Carbon*, 35 (5), 593-598(1997).

[22] Moreno-Castilla C., Lopez-Ramon M. V. and Carassco Marin F., Changes in surface chemistry of activated carbons by wet oxidation. *Carbon*, 38 (14), 1995-2000(2000).

[23] Sajjadi S., Mohammadzadeh A., Tran H., Anastopoulos I., Dotto G., Lopičić Z., Sivamani S., Rahmani-Sani A., Ivanets A. and Hosseini-Bandegharaei A., Efficient mercury removal from wastewater by pistachio wood wastes-derived activated carbon prepared by chemical activation using a novel activating agent. *J. Environ. Manage.*, 223 ,1001–1009(2018).

[24] Budinova T., Ekinci E., Yardim F., Grimm A., Björnbom E., Minkova V. and Goranova M., Characterization and application of activated carbon produced by H_3PO_4 and water vapor activation. *Fuel Process. Technol.*, 87 (10), 899-905(2006).

[25] Yorgun S., Vural N. and Demiral H., Preparation of high-surface area activated carbons from Paulownia wood by $ZnCl_2$ activation. *Microporous and Mesoporous Mater.*, 122 (3), 189-194(2009).

[26] Alcaraz L., Fernández A. and García-Díaz I., Preparation and characterization of activated carbons from winemaking wastes and their adsorption of methylene blue. *Adsorption Science & Technology*, 36(6), 1331-1341(2018).

[27] Aguilar C., Garc R., Soto-garrido G. and Arriagada R., Catalytic wet air oxidation of aqueous ammonia with activated carbon. *Appl. Catal. B Environ.*, 46(2), 229-237(2003).

[28] Zawadzki J., Infrared-spectroscopy in surface-chemistry of carbons. *Chem. Phys. Carbon.*, 21 ,147-380(1989).

[29] Puziy T.A.M., Poddubnaya O.I., Martinez-Alonso A., Suarez-Garcia F. and Tascon J.M.D., Characterization of synthetic carbons activated with phosphoric acid. *Appl. Surf. Sci.*, 200(4),196-202(2002).

[30] Prahas D., Kartika Y., Indraswati N.and Ismadji S., Activated carbon from jackfruit peel waste by H_3PO_4 chemical activation: Pore structure and surface chemistry characterization. *Chem. Eng. J.*, 140 (11), 32-42(2008).

[31] Bourbigot R.D. S. and Le Bras M., Carbonization mechanisms resulting from intumescence. Part II. Association with an ethylene terpolymer and the ammonium polyphosphate-pentaerythritol fire retardant system. *Carbon*, 33(3), 283-294(1995).

[32] Alghamdi A., Al-Odayni A., Saeed W., Al-Kahtani A., Alharthi F. and Aouak T., Efficient Adsorption of Lead (II) from Aqueous Phase Solutions Using

Polypyrrole-Based Activated Carbon. *Materials journal*, 12(12) (2019).
[33] Liu H., Wang X., Zhai G., Zhang J., Zhang C., Bao, N. and Cheng C., Preparation of activated carbon from lotus stalks with the mixture of phosphoric acid and pentaerythritol impregnation and its application for Ni(II) sorption. *Chem. Eng. J.*, 209, 155-162(2012).
[34] Chegrouche S., Mellah A. and Barkat M., Removal of strontium from aqueous solutions by adsorption onto activated carbon: kinetic and thermodynamic studies. *Desalination.*, 235(3), 306-318(2009).
[35] Lagergren S., About the theory of so-called adsorption of soluble substances, 1-39(1898).
[36] Hubbe M. A., Azizian S. and Douven S., Implications of apparent pseudo-second-order adsorption kinetics onto cellulosic materials: *A review. BioRes.*, 14(3), 7582-7626(2019).
[37] Weber W.J., Morris J.C., Kinetics of adsorption on carbon from solution, *J. Sanit. Eng. Div.*, 89(2),31-60(1963).
[38] Boyd G. E., Adamson A. W. and Myers L.S., The Exchange Adsorption of Ions from Aqueous Solutions by Organic Zeolites. II. Kinetics. *J. Am. Chem. Soc.*, 69(11), 2836-2848(1947).
[39] García-Díaz I., López F. and Alguaci F., Carbon Nanofibers: A New Adsorbent for Copper Removal from Wastewater. *J. Metals*, 8(11), 914(2018).
[40] Kilic M., Apaydin-varol E. and Pütün E., Adsorptive removal of phenol from aqueous solutions on activated carbon prepared from tobacco residues Equilibrium, kinetics and thermodynamics. *J. Hazard, Mater*, 189 (2), 397-403(2011).
[41] Reichenberg D., Ion-Exchange Resins in Relation to their Structure. III. Kinetics of Exchange, *J. Am. Chem. Soc.* 75(3), 589-597(1953).
[42] Giles C.H., Pacewan T.H., Nakhwa S.N. and Smith, D., Studies in adsorption. Part XI. A system of classification of solution adsorption isotherms, and its use in diagnosis of adsorption mechanisms and in measurement of specific surface areas of solids. *J. Chem. Soc.*, 786, 3973-3993(1960).
[43] Langmuir I., The adsorption of gases on plane surfaces of glass, mica and platinum. *J. Am. Chem. Soc.*, 40, 1361-1403(1918).
[44] Husein D.Z., Adsorption and removal of mercury ions from aqueous solution using raw and chemically modified Egyptian mandarin peel using raw and chemically modified Egyptian mandarin peel. *Desalin. Water Treat.*, 51 (35), 6761-6769(2013).
[45] Weber R.K., Chakraborti T.W., Pore and Solid Diffusion Models for Fixed Bed Adsorbents. *J. Am. Inst. Chem. Eng.*, 20 (2), 228-238(1974).
[46] Freundlich H.M.F., Over the Adsorption in Solution. *J. Phys. Chem.*, 57, 385(1906).
[47] Zhang F., Nriagu J.O. and Itoh H., Mercury removal from water using activated carbons derived from organic sewage sludge. *Water Res.*, 39 (3), 389-395(2005).
[48] Youssef A.M., Hassan A.F., Ebiad M.A. and Bakry M.B., Adsorption of Hg2+ using modified sulfur-impregnated activated carbon from olive stone. *Mansoura J. Chem.*, 42 (1) 1-15(2016).
[49] Jedrzejewski R., Lendzion-Bielun Z., Reduction Process of Iron Catalyst Precursors for Ammonia Synthesis Doped with Lithium Oxide. *J. Catalysts*, 8(11), 494-503(2018).
[50] Kim Y., Kim C., Yi J., Arsenic Removal Using Mesoporous Alumina Prepared via a Templating Method. *Environ. Sci. Technol.*, 38 (3), 924-931(2004).
[51] Abdelsamad A. A., Abdel Aal M. M., Haggag E. A. and Yosef W. M., Synthesis and Characterization of Functionalized activated Carbon for Removal of Uranium and Iron from Phosphoric Acid, *Journal of Basic and Environmental Sciences*, 7, 140-153(2020).
[52] Mahmoud M. A., Gawad E. A., Hamoda E.A. and Haggag E. A., Kinetics and Thermodynamic of Fe (III) Adsorption Type onto Activated Carbon from Biomass: Kinetics and Thermodynamics Studies. *J. of Environmental Science*, 11(4), 128-136(2015).
[53] Dacrory S., Haggag E. A., Masoud A. M., Abdo S. M., Eliwa A. A. and Kamel S., Innovative Synthesis of Modified Cellulose Derivative as a Uranium Adsorbent from Carbonate Solutions of Radioactive Deposits. *Journal of Cellulose*, 27, 7093-7108(2020).
[54] Khawassek Y. M., Eliwa A. A., Haggag E. A., Omar S. A. and Mohamed S. A., Adsorption of rare earth elements by strong acid cation exchange resin thermodynamics, characteristics and kinetics. *SN Applied Sciences*, 1,51(2019).
[55] Khawassek Y. M., Eliwa A. A., Haggag E. A., Mohamed S. A and Omar S. A., Equilibrium, Kinetic and Thermodynamics of Uranium Adsorption by Ambersep 400 SO_4 Resin. *Arab Journal of Nuclear Sciences and Applications*, 50(4), 100-112(2017).
[56] Haggag E. A., Abdelsamad A. A. and Masoud A. M., Potentiality of Uranium Extraction from Acidic Leach Liquor by Polyacrylamide-Acrylic Acid Titanium Silicate Composite Adsorbent. *International Journal of Environmental Analytical Chemistry*, 100(2), 204-224(2019).
[57] Alex Marchenko A., Truflandier L. and Autschbach J., Uranyl Carbonate Complexes in Aqueous Solution and Their Ligand NMR Chemical Shifts and 17O Quadrupolar Relaxation Studied by ab Initio Molecular Dynamics. *Inorg. Chem.*, 56(13), 7384–7396(2017).
[58] AbdelAal M. M. and AbdelSamad A. A. Comparative Chemical Studies Between Fixed Bed and Batch Dynamic Ion Exchange Techniques for Extraction of Uranium. *Arab J. Nucl. Sci. Appl.*, 52(2), 187-200(2019).
[59] Masoud A. M., Sorption behavior of uranium from Sulfate media using purolite A400 as a strong base anion Exchange resin. *International Journal of Environmental Analytical Chemistry*, 2020.
[60] Masoud A. M., Youssef W.M., Massoud A. A., Sorption Characteristics of Uranium from Sulfate Leach Liquor by commercial strong base anion exchange resins. *Journal of Radioanalytical and Nuclear Chemistry*, (2019).
[61] El-Sheikh A. S., Haggag E. A. and Abd El-Rahman N. R., Adsorption of Uranium from Sulfate Medium Using a Synthetic Polymer; Kinetic Characteristics. *Radiochemistry*, 62(4), 499–510(2020).
[62] Abderrahim O., Didi M.A. and Villemin D., A new sorbent for uranium extraction polyethyleniminephenylphosphonamidic acid. *J. Radioanal Nucl Chem.*, 279, 237–244(2009).

[63] Metildaa P., Sanghamitrab K., Mary Gladisa, J., Naidub G.R.K. and Prasada Rao T., Amberlite XAD-4 functionalized with succinic acid for the solid phase extractive preconcentration and separation of uranium (VI). *Talanta*, 65(1),192–200(2005).
[64] Venkatesan K. A., Sukumaran V., Antony M. P. and Vasudeva Rao P. R., Extraction of uranium by amine, amide and benzamide grafted covalently on silica gel. *J. Radioanal Nucl Chem.*, 260, 443–450 (2004).
[65] Camacho L.M., Deng S. and Parra R.R., Uranium removal from groundwater by natural clinoptilolite zeolite: effects of pH and initial feed concentration. *J Hazard Mater.*, 175, 393–398(2010).
[66] Youssef W. M., Hagag M. S.and Ali A. H., Synthesis, characterization and application of composite derived from rice husk ash with aluminium oxide for sorption of uranium. *J. Adsorption Science & Technology*, 1-20(2018).

Arabic summary

الملخص باللغة العربية

تم تصنيع الكربون عالي المسامية المنشط بالفوسفور والمشتق من قشر الفستق((PNS كمواد ماصة محتملة لليورانيوم السداسى من وسط الكبريتات الحامضى. تم تصوير الكربون المنشط الفوسفاتي المحضر (PAC) باستخدام SEM ، TEM والذي أظهر بنية مسامية للغاية. تم دراسة استخلاص اليورانيوم السداسى من الوسط الحمضي باستخدام (PAC) ودراسة العديد من العوامل مثل الرقم الهيدروجيني ووقت التلامس الاتزانى ونسبة السائل إلى المادة الصلبة وتركيز اليورانيوم السداسى الأولية. في ظل الظروف المذكورة ، تم العثور على درجة الحموضة المثلى لامتصاص اليورانيوم السداسى لتكون 3.5. تم العثور على قدرة امتصاص اليورانيوم على (PAC) في الظروف المثلى لتكون 335 مجم / جم. تم تطبيق النتائج التجريبية على نماذج حرارية لانجموير وفريوندليش وتيمكين ودوبينين-رادوشكيفيتش. تم تحديد ثابت التوازن الديناميكي الحراري والطاقة الحرة ° ΔG من -4.72 إلى - 7.65 مول/كيلو جول. وأظهرت النتائج الطبيعة التلقائية لعملية الامتزاز. تم وصف بيانات الخواص الحركية بشكل أفضل من خلال نموذج الدرجة الثانية الزائف.